Hindawi
Geofluids
Volume 2022, Article ID 3541528, 14 pages
https://doi.org/10.1155/2022/3541528

Research Article

Research on Hanger Force and Main Arch Stability of Long-Span Concrete-Filled Steel Tube Arch Bridge

Yanli Wu,[1] **Mowei Qiu**,[1] **Shaokun Ma**,[2] **Xinlei Gao**,[3] **and Yahong Han**[3]

[1]*Huanghe Jiaotong University, Wuzhi, Henan 454950, China*
[2]*School of Civil Engineering, Guangxi University, Nanning 530004, China*
[3]*Harbin Institute of Technology National Engineering Research Center of Urban Water Resources Co., Ltd., Harbin 150006, China*

Correspondence should be addressed to Yanli Wu; 2013100221@zjtu.edu.cn

Received 28 February 2022; Revised 7 July 2022; Accepted 19 July 2022; Published 5 August 2022

Academic Editor: Dan Ma

In recent years, the construction of a CFST arch bridge has developed rapidly; however, as a kind of structural system dominated by compression, with the increase of material strength and span, the stability of the main arch of the CFST arch bridge has become more and more important. In this paper, the finite element method is used to analyze the hanger force and the main arch stability of the long-span CFST arch bridge. Combined with the Shenzhen Rainbow Bridge project, the axial force of the hanger, the internal force, and stability of the main arch of the arch bridge are studied. In the establishment of the finite element model, considering the actual operation of the arch bridge, the model simulates the interaction between steel pipe and concrete, it studies the large deformation of CFST arch bridges, and the stress distribution and overall stability of the arch bridge are analyzed. The results show that the main deformation of the CFST arch bridge is the vertical displacement of the deck, and the axial force of most members of the upper arch ribs is greater than that of the lower arch ribs. The axial force and bending moment of the lower arch rib near the arch foot are larger, and the compressive stress of the arch foot is greater than that of other positions. The axial force of the suspender of the arch bridge is the largest at both ends of the hanger and the middle hanger, and the axial force of the other hanger is close to each other, and the axial force changes little under the same case. The buckling modes of the arch are mainly the lateral buckling or flexural buckling of the arch rib outside the plane, which indicates that the vertical stiffness of the arch bridge structure is larger than that of the transverse stiffness. The research results make the load-bearing mechanism of the CFST arch bridge more clear and also provide a certain reference for the design and construction of the CFST arch bridge.

1. Introduction

The strength and performance of steel tube and concrete in the CFST arch bridge should be supplemented and improved [1]. First, the steel tube wall is reinforced by filling it with concrete [2]. Secondly, with the help of the steel tube's hoop effect on the core concrete, the core concrete is in a three-way compression state, so that the core concrete has higher compressive strength and antideformation ability, thus greatly improving the bearing capacity of the arch rib [3]. In addition, the steel tube ribbed arch can make the main arch ring itself a template for a self-erecting system and pouring concrete in the tube, which is convenient for the realization of the construction without support, thus solving the two major problems of the application and construction of the high strength material of the arch bridge [4]. And its economic benefits are more in line with the existing national conditions of our country, and it has become a new hot bridge type and is considered to be a relatively ideal structure for the construction of long-span arch bridges [5]. For the structure of the CFST arch bridge, the stability problem is particularly prominent, as the structure of the arch bridge is more complex; once the instability failure occurs, it will cause a chain reaction, resulting in huge losses. The stress of the CFST arch bridge is complicated, and it is difficult to calculate with the existing analytical methods, the finite element method is an effective method to solve complex problems, so the finite element method to analyze

the stability of the CFST arch bridge has the value of popularization and application.

The stability of long-span CFST arch bridges has been studied by many scholars at home and abroad. In order to study the structural stability and dynamic performance of the long-span CFST arch bridge, from the design form of the arch bridge hanger and different dynamic models, the influence line characteristics of the tie arch bridge and impact coefficient of bridge span under different train excitation are studied [6]. Some scholars have studied the influence of different filling schemes on the stability of CFST arch bridges from the perspective of construction [7]. For in-plane stability of a single round tubular concrete-filled steel tube arch bridge, considering the effects of equivalent slenderness ratio, span ratio, and longitudinal stiffness, the ultimate bearing capacity coefficient of the arch bridge is calculated [8]. The homogeneous generalized yield function for the compression and flexural stability analysis of CFST members was established by a comprehensive test method and regression analysis method; using a linear elastic iterative method to calculate the ultimate bearing capacity of the structure, it overcomes the limitation of the incremental nonlinear finite element method and can obtain higher calculation accuracy and efficiency [9]. Some scholars have studied the stability of the inclined concrete-filled steel tube arch bridge, the inclined arch can significantly improve the stability of the arch rib, but the bearing capacity of the arch rib should be matched with the CFST arch rib, so as not to be destroyed and lead to the overall instability of the arch rib under the ultimate load [10]. In order to study the influence of transverse braces on the concrete-filled steel tubular arch bridge, the effect of the parameters such as the spacing of transverse braces, the type of transverse braces, and the stiffness of transverse braces on the transverse elastic stability of the arch bridge is determined, and the main factors affecting the transverse stability of the arch bridge are judged [11]. In addition, the stability of the CFST arch bridge is also related to the research method, the characteristics of bridge foundation rock, and the underground water level [12–15].

2. Stability Theory Overview of CFST Arch Bridge

For CFST arch bridges, the bearing capacity of the main arch is mainly determined by its strength and stability, especially the stability, which has an important influence on the ultimate bearing capacity of CFST arch bridges. The buckling of the main arch can be divided into two types: branch point buckling and extreme point buckling.

2.1. Branch Point Buckling. Branch point buckling usually refers to the stressed structure being a perfect system; that is, the geometric shape and stress state of the arch are idealized, without defects and deviations, and the critical load of the arch can be solved by an analytical method:

$$N_{cr} = \pi^2 \frac{EI}{(kS)^2}. \quad (1)$$

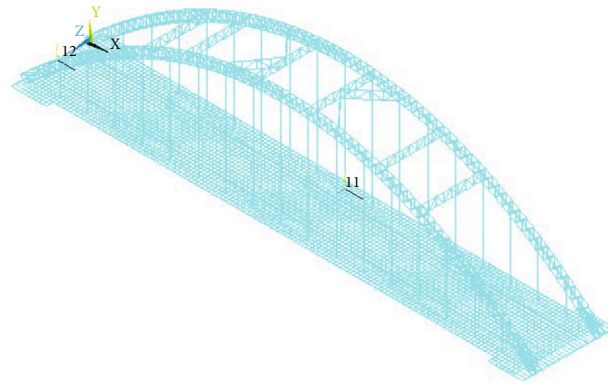

Figure 1: The finite element calculation model of CFST arch bridge.

In the equation, N_{cr} is a quarter of the cross-critical axial load of the arch, E is the elastic modulus of material, I is the moment of inertia of cross-section, S is half the length of the arch axis, and k is an effective length coefficient.

The critical load of branch point buckling can also be solved by the finite element method; usually using the virtual work principle, listing the equilibrium conditions, the element stiffness matrix of the structure is calculated and combined with the boundary conditions and load distribution of the arch. The equations of rod end displacement and rod end force are given by integrating the positioning vector and the overall stiffness matrix; the critical load and buckling mode of the arch branch point can be solved by the condition of a nonzero solution of joint displacement.

2.2. Extreme Point Buckling. Extreme point buckling generally occurs in imperfect systems; this is mainly due to the deviation of the geometry of the structure, uneven material properties, asymmetric load distribution, and other factors resulting in the buckling problem. At this time, the arch is in the state of bending and pressing, and the coupling problem between geometric nonlinearity and material nonlinearity needs to be considered simultaneously, which is very complicated to calculate. Especially for a concrete-filled steel tube arch bridge, the main arch belongs to a composite material, and the structural material property is complex, which makes the calculation of the stability of the main arch more difficult. The finite element method is generally used to calculate the buckling load of the main arch.

3. Finite Element Model

3.1. Material Parameters. In the calculation model, the constitutive relation of the CFST of the main arch is the key problem to establish the finite element model. At present, there are three methods to treat the CFST constitutive materials in China: the same node double element method, the equivalent stiffness method, and the unified theory method [16]. The equivalent stiffness method is relatively simple in modeling, and the accuracy can meet the engineering requirements when carrying out static force, but it does not consider the tightening effect of steel pipe on core

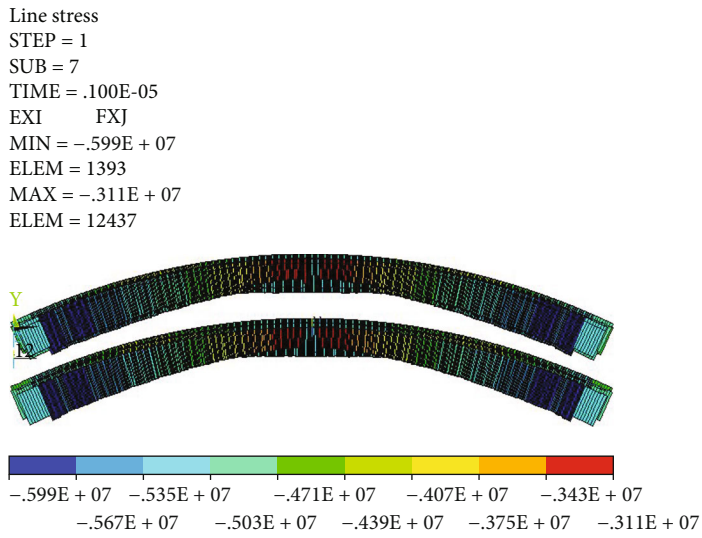

Figure 2: The axial force cloud map of main arch under case 5 (N).

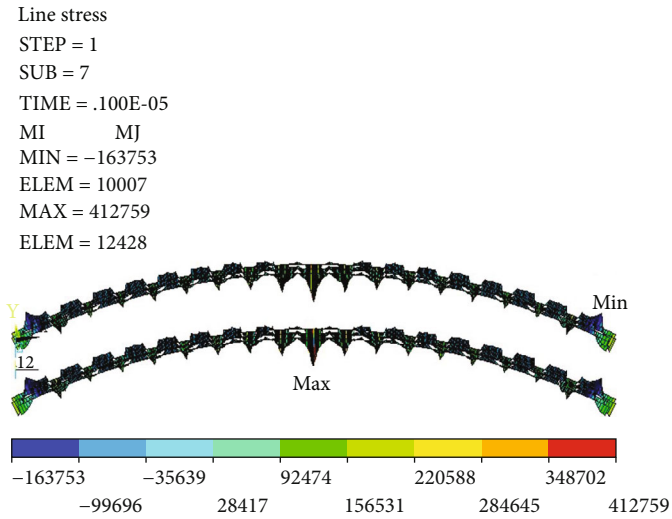

Figure 3: The bending moment cloud map of main arch under case 5 (N·m).

concrete [17]. According to the equivalent stiffness method, the comprehensive elastic modulus, area, and moment of inertia of CFST members in the limit state of normal service are calculated as follows.

The compression and tensile stiffness are

$$EA = E_a A_a + E_c A_c. \tag{2}$$

The bending stiffness is

$$EI = E_a I_a + E_c I_c. \tag{3}$$

In the expression, A_a and I_a are, respectively, the area of the cross-section of the steel tube and the moment of inertia with respect to its barycenter axis; A_c and I_c are, respectively, the area of the cross-section of concrete in the steel tube and the moment of inertia with respect to its barycenter axis; and E_a and E_c are the elastic modulus of steel and concrete, respectively.

The parameter setting of the arch bridge will affect the finite element simulation results, and the bridge stiffness will affect its deformation and vibration frequency. A bridge with high stiffness will produce small deformation and high frequency. In addition, the elastic modulus and Poisson's ratio of the material also affect the stress of the bridge.

3.2. Project Summary. Shenzhen Rainbow Bridge is 1.2 km long; it spans 29 railway channels of Shenzhen North Railway Station, making it one of the most bridges across railway channels in the world. The main bridge is a bottom-mounted CFST flexible tie arch with no thrust at the arch foot, the width of the bridge deck is 23.5 m, and the width of the bridge deck at the arch foot is 28 m. Computational span is 150 m, single span two-way four lanes, the rise-span ratio is 1/4.5, the arch axis is a catenary arch axis,

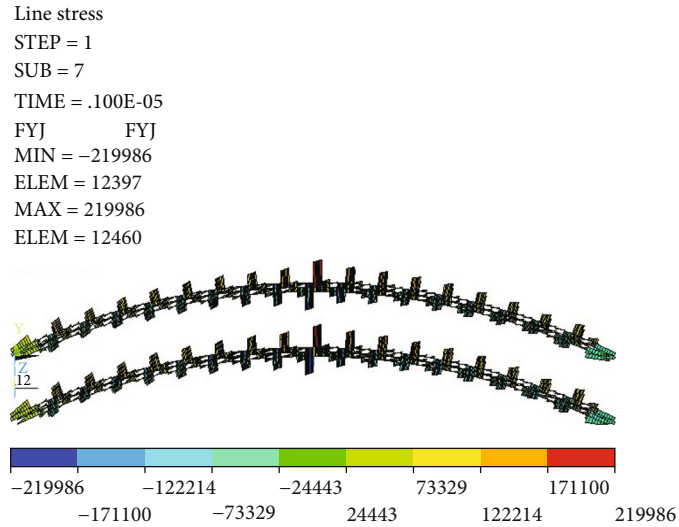

Figure 4: The shear force cloud map of main arch under case 5 (N).

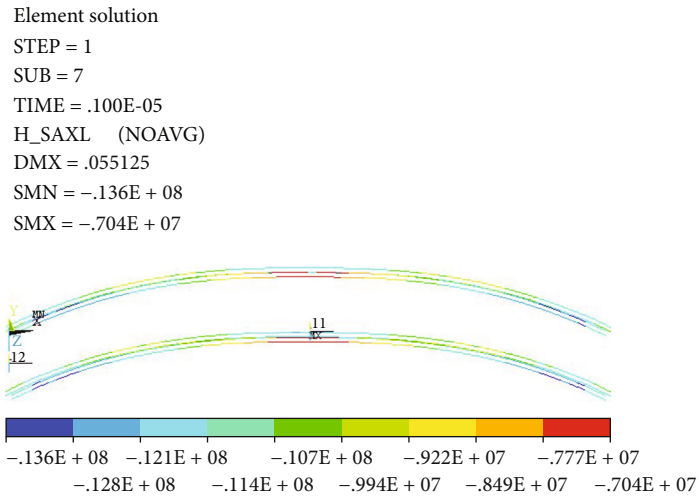

Figure 5: The axial stress cloud map of main arch under case 5 (Pa).

and the arch axis coefficient is 1.167. The bridge has double arch ribs, each arch rib is composed of $4\phi750 \times 12$ mm steel tube truss section, truss height is 3.0 m, truss width is 2.0 m, and the steel tube is filled with No.50 microexpansion concrete. A total of 17 pairs of hanger rods are set up in the arch ribs of the bridge, the hanger rods at each point are double hanger rods, and the hanger cables are extruded double-layer large pitch twisted stay cables [18]. Each hanger cable is composed of 61 galvanized high strength and low relaxation prestressed steel wires with a diameter of 7 mm; the standard strength of the steel wire is $R_y^b = 1670$ MPa. The foundation of the substructure is a single-column single-pile type, and the piers are composed of CFST columns with a diameter of 2.8-3.4 m with variable sections. The main arch and bridge pier adopt the form of arch pier consolidation, and the arch foot is the intersection point of the main arch pad, pier top, cap beam, and horizontal tie rod. The elastic modulus of steel wire $E_s = 205$ GPa, the steel bar uses HRB400, its strength design value is $f_y = f_y' = 360$ MPa, concrete strength grade is C50, and its elastic modulus is $E_c = 34.5$ GPa. The stability of the arch bridge is calculated by a linear elastic constitutive equation.

3.3. Finite Element Model. The bridge is modeled by general finite element software ANSYS; the model is divided into 56,387 elements and 510,998 nodes. The arch ribs of the bridge are modeled according to the arch axis equation, and the upper and lower strings of CFST are discretized by three-dimensional elastic beam elements; it is a uniaxial force element which can be used to bear pull, pressure, bending, and torsion and endows it with the characteristics of simulating CFST [19]. In addition, the BEAM4 beam element is also used to simulate the upper and lower horizontal joints, vertical belly bars, oblique belly bars, wind braces, and the longitudinal beams, beams, and precast hollow slabs in the bridge deck system. The suspender and the longitudinal

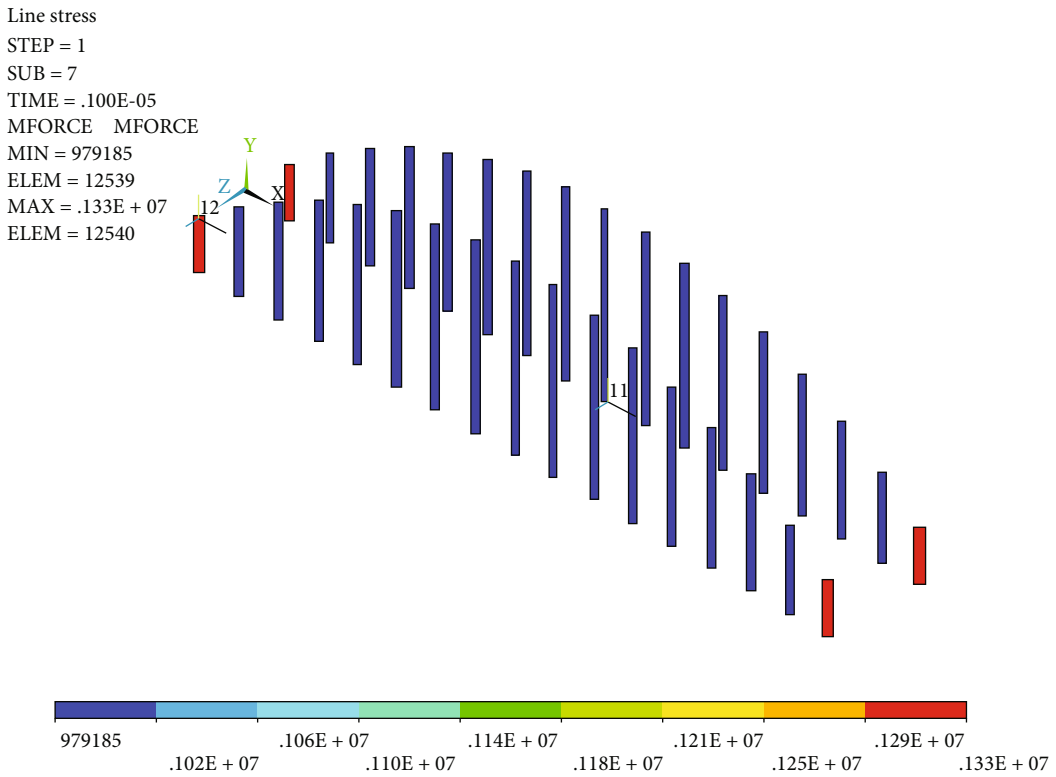

Figure 6: The axial force cloud map of hanger under case 1 (N).

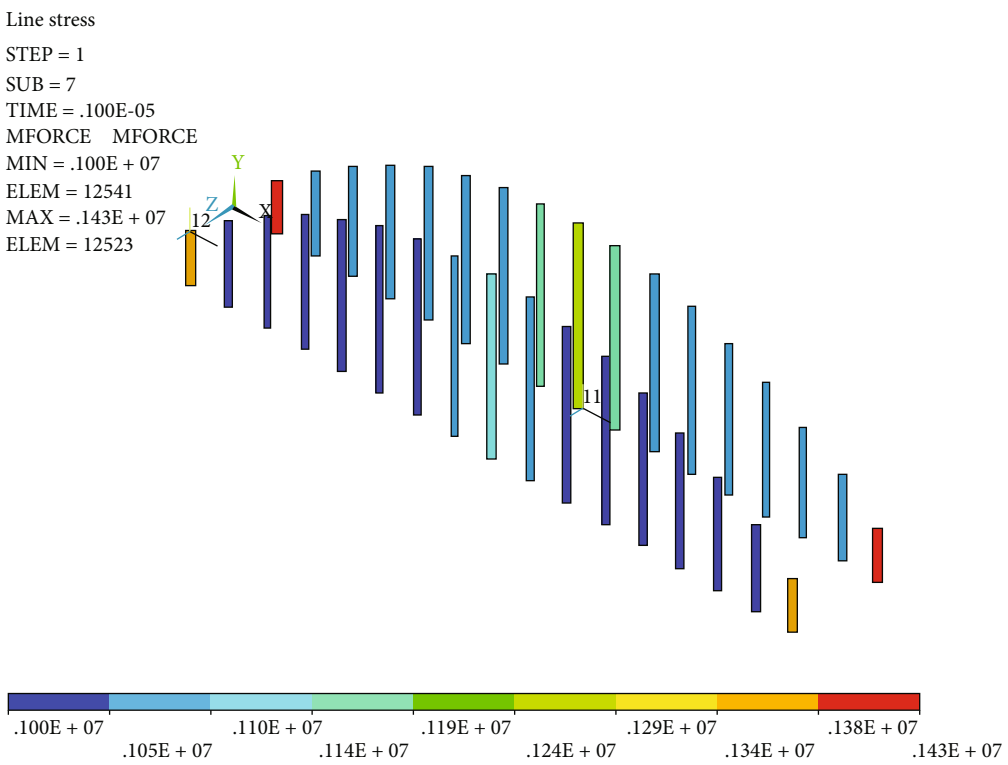

Figure 7: The axial force cloud map of hanger under case 2 (N).

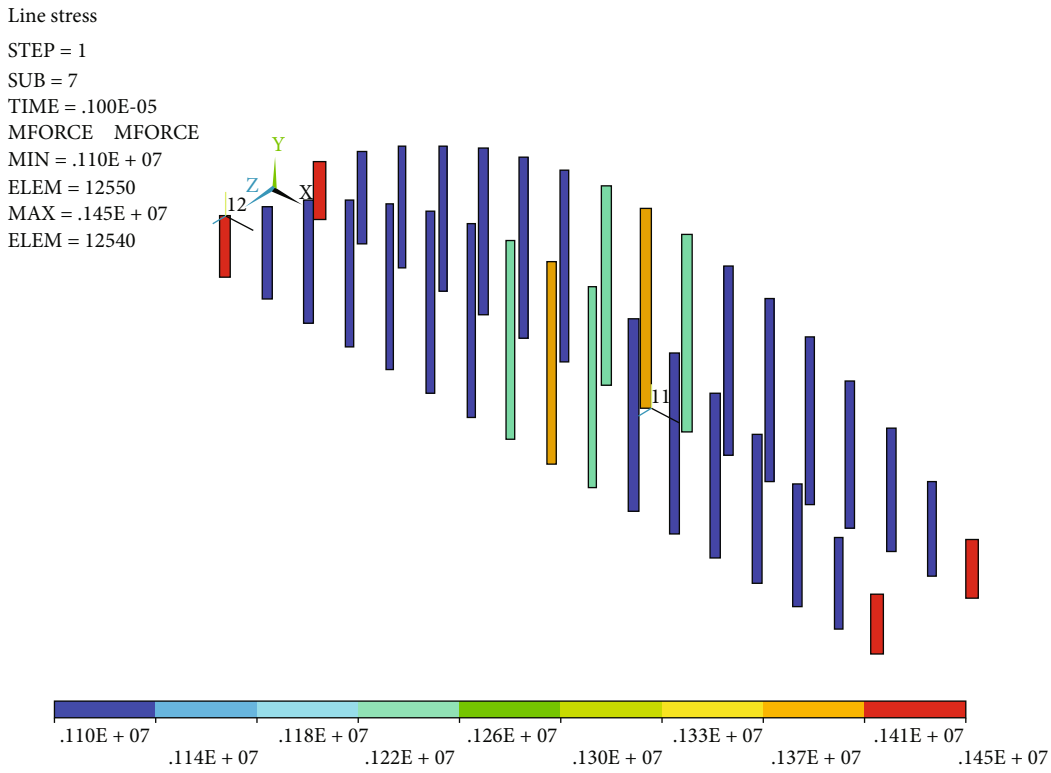

Figure 8: The axial force cloud map of hanger under case 5 (N).

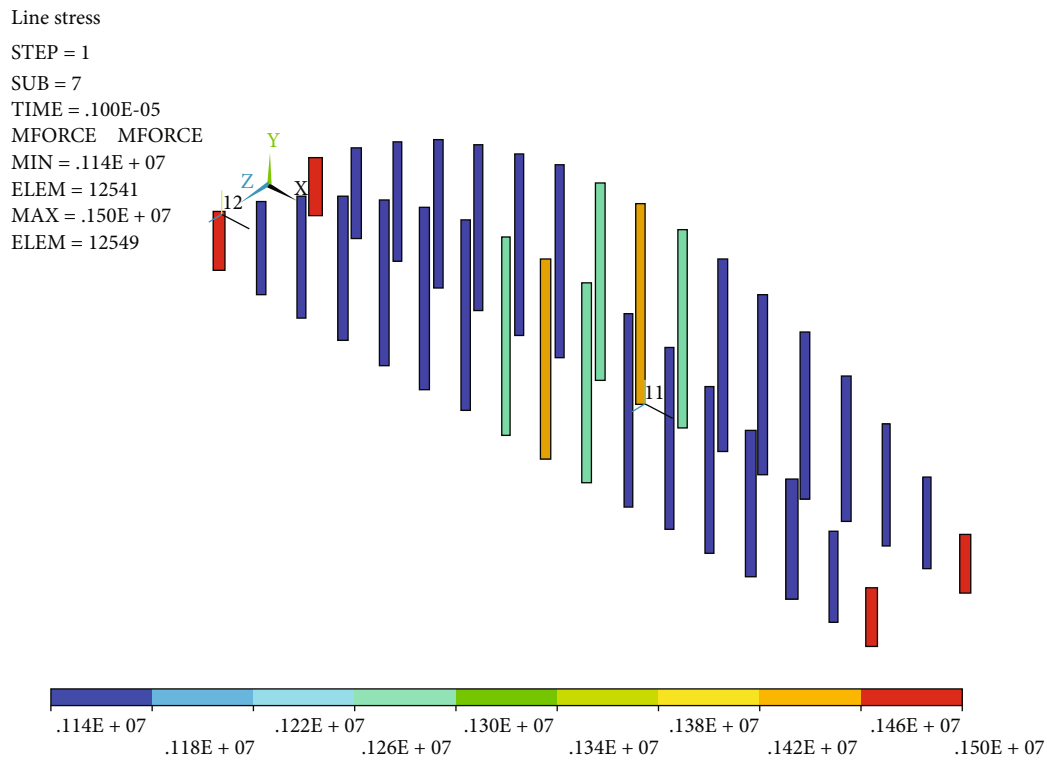

Figure 9: The axial force cloud map of hanger under case 7 (N).

horizontal tie rod are simulated by the space rod element (Link10) which only bears tension, and the element characteristics are set to only bear tension. The applied prestress is simulated by the method of equal effect variation. The principle is to generate the strain equivalent to the prestress in the structure by defining the real constant of the structure,

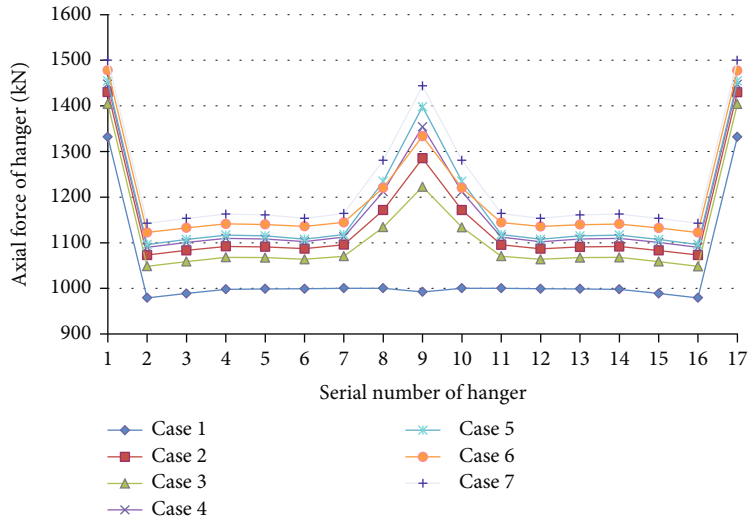

Figure 10: The variation curve of hanger axial force on the north side of arch bridge under various cases.

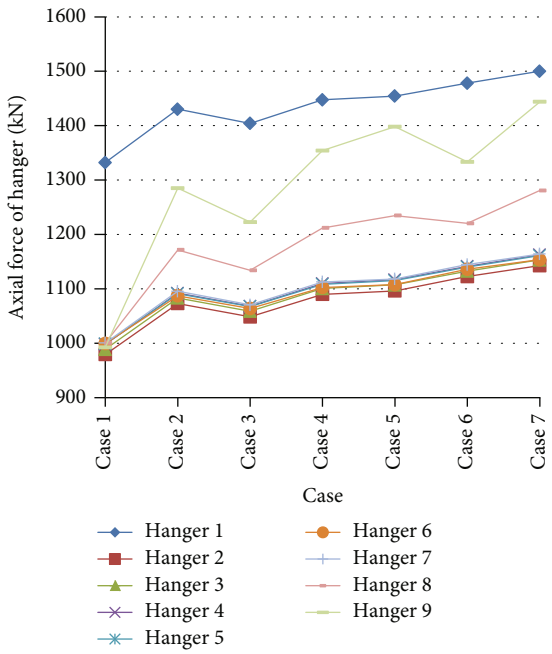

Figure 11: The variation curve of hanger axial force on north side of arch bridge with cases.

so as to achieve the purpose of indirect application of prestress [20]. The calculation model takes into account the bond between steel pipe and concrete; the connection between the main arch, suspender, and bridge slab; the structural constraints of the arch bridge; and the load during the construction and operation of the arch bridge. The finite element calculation model of the CFST arch bridge is shown in Figure 1.

3.4. Calculation Cases. In order to study the hanger force and the stability of the main arch of the CFST arch bridge, the rainbow bridge deck is arranged as four lanes in both directions, the lane load is 10.5 kN/m, and the crowd load is 2.5 kN/m^2. According to the volume and bulk density of the element, the weight of the bridge member is exerted on the element in the form of physical force; according to the principle of static equivalence, the variable loads of bridges are converted into uniform loads acting on the corresponding longitudinal beam elements. According to the stress characteristics of the arch bridge in operation and the layout of the driveway, when vehicles cross the bridge, considering the influence line of the bridge bending moment, the bridge weight, lane load, and crowd load are combined. The calculation conditions are combined as follows: case 1, weight of bridge structure; case 2, weight + 0.7 × lane 1 + 0.7 × lane 2; case 3, weight + 0.7 × lane 1 + 0.7 × lane 3; case 4, weight + 0.7 × lane 1 + 0.7 × lane 2 + 0.7 × lane 3; case 5, weight + 0.7 × lane 1 + 0.7 × lane 2 + 0.7 × lane 3 + 0.7 × lane 4; case 6, weight + 0.7 × lane 1 + 0.7 × lane 2 + crowd load 1; and case 7, weight + 0.7 × lane 1 + 0.7 × lane 2 + 0.7 × lane 3 + 0.7 × lane 4 + crowd load 1 + crowd load 2.

4. Force Analysis of Arch Bridge Structure

In order to have a clear understanding of the stress of the CFST arch bridge, a three-dimensional finite element model of the arch bridge is established based on the actual situation of the arch bridge. In the model, the bond between steel tube and concrete is simulated; the equivalent stiffness of CFST is given; the connection between the main arch, suspender, and bridge slab is simulated; and the element type used in the model of the CFST arch bridge is determined. Considering the load combination and the corresponding boundary conditions, the internal force of the suspender and the stability of the main arch of the CFST arch bridge are analyzed.

4.1. Force Analysis of Main Arch. Through the finite element analysis of the CFST arch bridge, the internal force and stress cloud maps of the main arch under various cases are obtained. The internal force and stress cloud maps of the main arch under case 5 are shown in Figures 2–5.

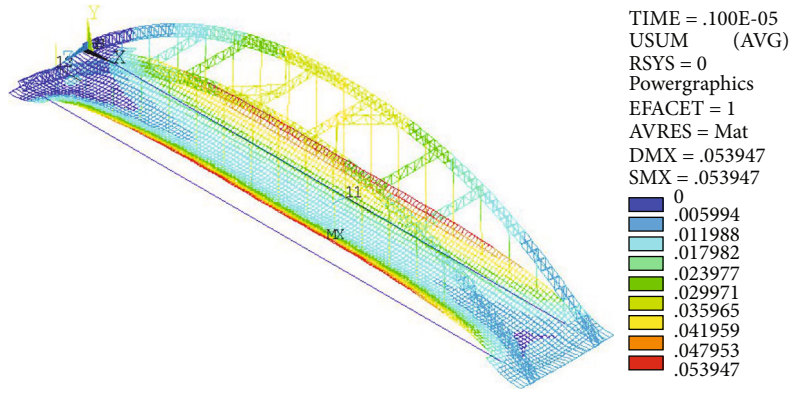

Figure 12: The overall displacement cloud map of arch bridge under case 1 (m).

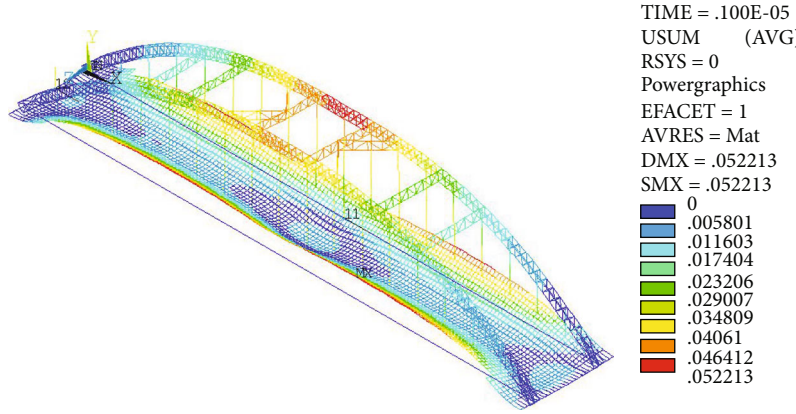

Figure 13: The overall displacement cloud map of arch bridge under case 2 (m).

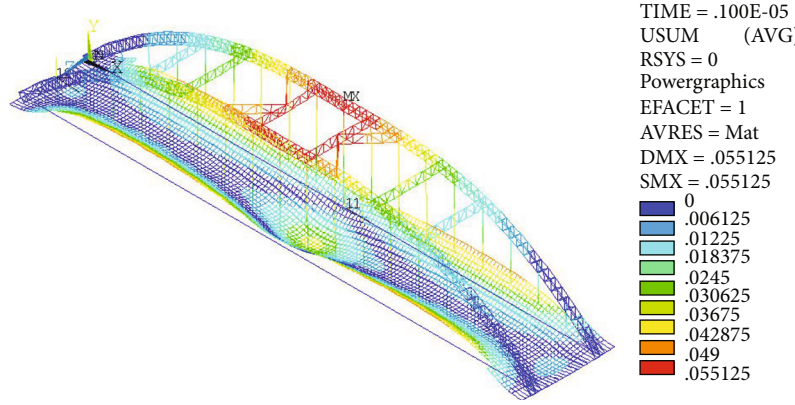

Figure 14: The overall displacement cloud map of arch bridge under case 5 (m).

As we can see from Figure 2, the whole CFST of the arch rib is in the state of compression and increases with the increase of load. The absolute value of the axial force in the middle part of the arch rib is small but increases obviously to both sides, and the maximum value of the absolute value of the axial force appears near the arch foot. In Figure 3, the maximum positive bending moment is 412.759 kN·m; the maximum negative bending moment is -163.753 kN·m. In Figure 4, the shear force in the arch rib changes at the hanger, which is due to the effect of the transmission force of the hanger, and the maximum and minimum values appear at the relatively symmetrical position in the middle of the span. In Figure 5, the axial stress of the four upper and lower string CFST in the arch rib is in a regular distribution from the top to the foot, the maximum value is 13.6 MPa, stress is less than the axial compressive strength of C50 microexpansion concrete 23.1 MPa, and the upper arch rib compressive stress is greater than the lower chord compressive stress.

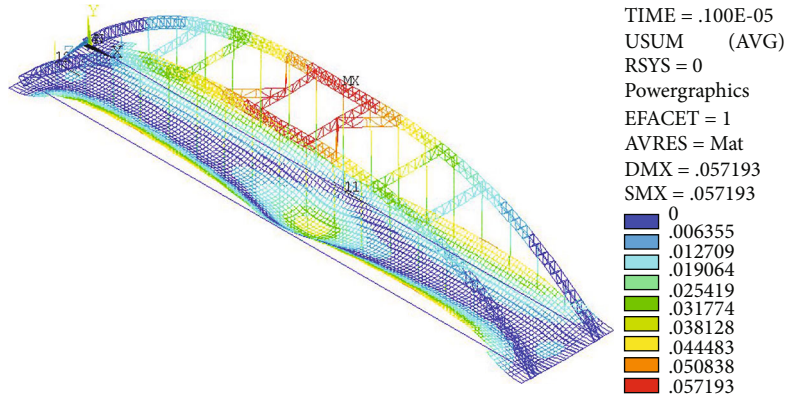

Figure 15: The overall displacement cloud map of arch bridge under case 7 (m).

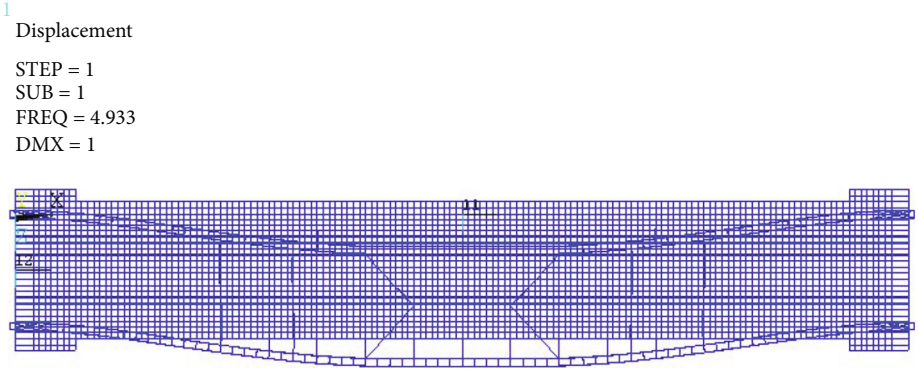

Figure 16: The first order buckling mode of arch bridge under case 1.

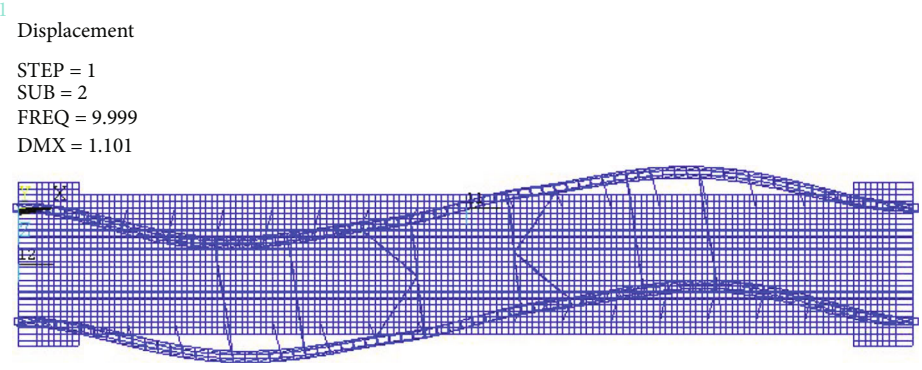

Figure 17: The second order buckling mode of arch bridge under case 1.

4.2. Force Analysis of Hanger. Through the finite element analysis of the CFST arch bridge, the axial force of the hanger under various cases is obtained. The axial force cloud map of the arch bridge hanger under cases 1, 2, 5, and 7 is shown in Figures 6–9.

We can see from Figures 6–9, under case 1, that the hanger is the main tensile component in the bridge, its main function is to transfer the weight and load of the bridge deck to the arch ribs, so its stress is large. Under case 2, compared with case 1, the axial force of each hanger varies greatly, and the force is no longer uniform, the hanger force at the middle and end of the span is larger, and the hanger force at the north side is obviously larger than that at the south side, but it still presents longitudinal symmetry. Under case 5, due to the symmetry of the lane, the force of the hanger is also symmetrical, the distribution law of the hanger force between the middle and the end of the span is larger, and the hanger force between them is smaller. Under case 7, the tension of the hanger increases obviously with the increase of the distribution load, the stress of the hanger at the end is larger, and the stress of the other hanger near the end is relatively small, with the maximum value of 1500 kN.

In order to analyze the axial force of the hanger of the arch bridge, the northern hanger of the arch bridge is numbered from one end of the arch bridge to the other end, and the numbers are 1 to 17. The variation curve of the hanger

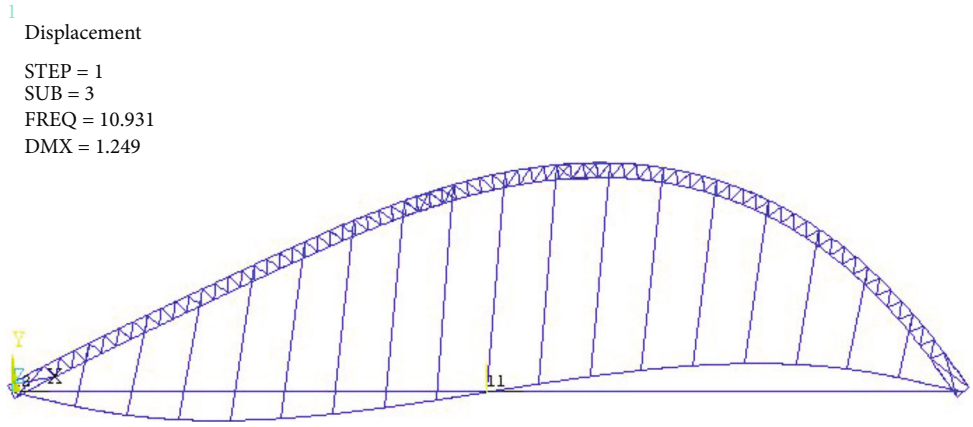

Figure 18: The third order buckling mode of arch bridge under case 1.

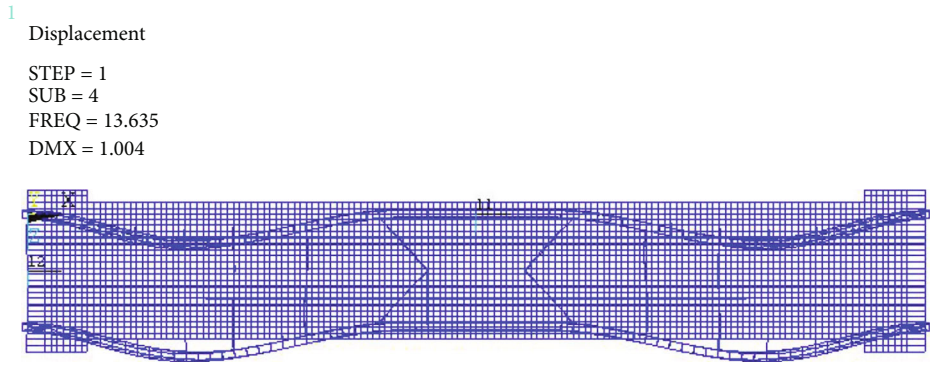

Figure 19: The fourth order buckling mode of arch bridge under case 1.

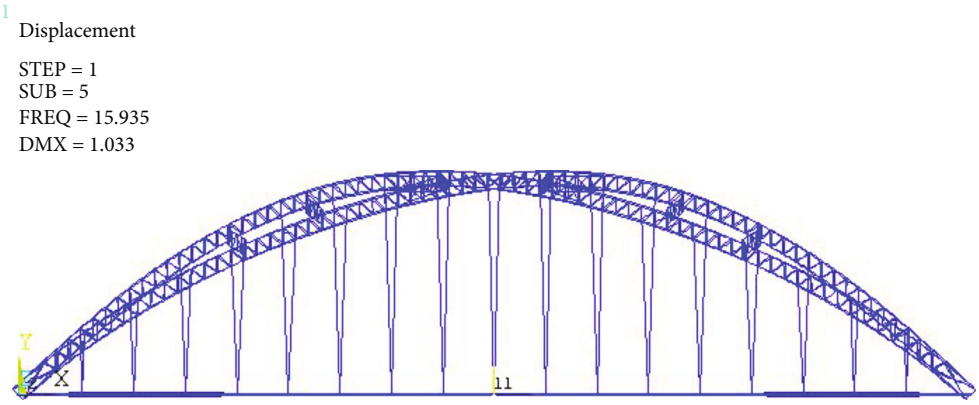

Figure 20: The fifth order buckling mode of arch bridge under case 1.

axial force on the north side of the arch bridge under various cases is shown in Figure 10; the variation curve of hanger axial force on the north side of the arch bridge with cases is shown in Figure 11.

We can see from Figure 10 that the axial force of the hanger on the north side of the arch bridge changes symmetrically; except for case 1, the axial force of the hanger on both ends and the middle suspender is the largest in all cases; the axial force of hanger 2 to hanger 5 and hanger 11 to hanger 16 has little change and tends to be stable. Under case 1, the axial force of the hanger at both ends is the largest, while the axial force of the hanger in the middle tends to be stable with little change. The maximum axial force of the hanger at both ends appears in case 7, and the maximum axial force value is 1500 kN. The maximum axial force of the middle hanger appears in case 7, and the maximum axial force value is 1443.8 kN. We can see from Figure 11 that due to the symmetry of the axial force of the hanger, only hanger 1 to hanger 9 are taken; under various cases, the axial force of hanger 1 is the largest, and it shows a trend of gradual increase with each case. The axial force of hanger 8 and hanger 9 fluctuates with the case, the

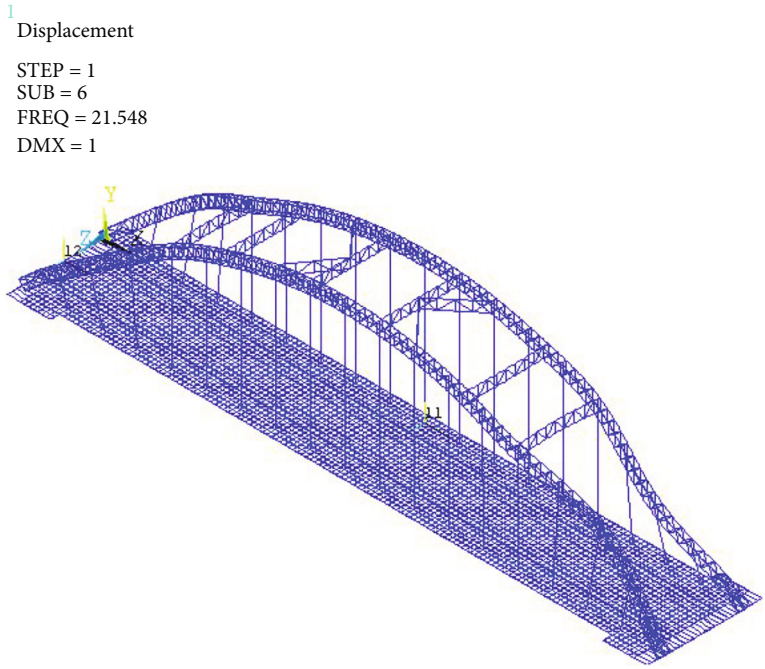

Figure 21: The sixth order buckling mode of arch bridge under case 1.

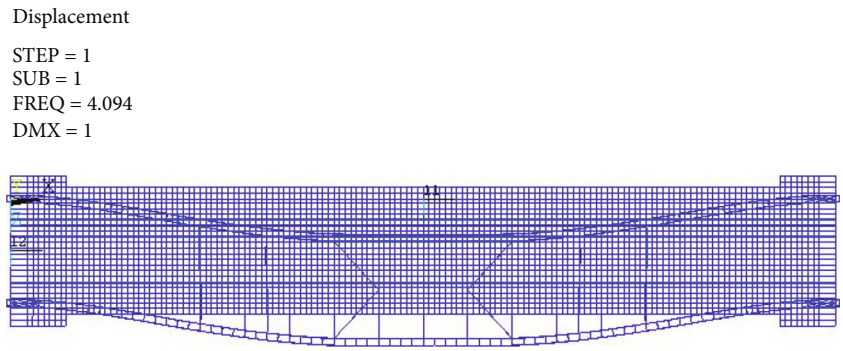

Figure 22: The first order buckling mode of arch bridge under case 7.

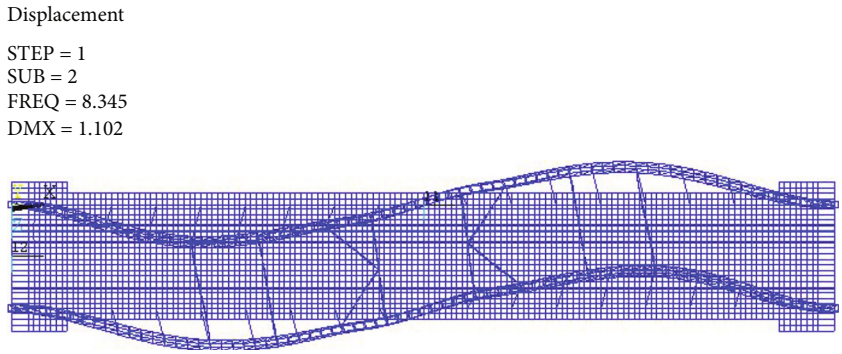

Figure 23: The second order buckling mode of arch bridge under case 7.

axial force values of other hangers are very close, and the axial force changes little under the same case. Under case 7, the axial force of each hanger is the maximum.

4.3. Displacement Analysis. Through the numerical simulation analysis of the CFST arch bridge, the overall displacement of the arch bridge under various cases is obtained.

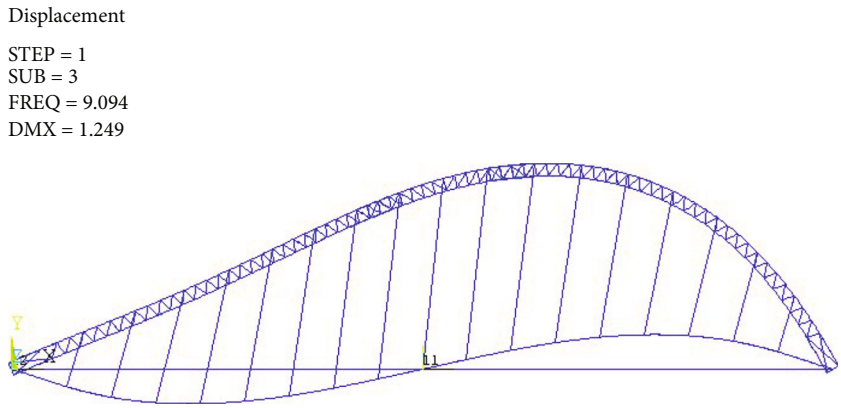

Figure 24: The third order buckling mode of arch bridge under case 7.

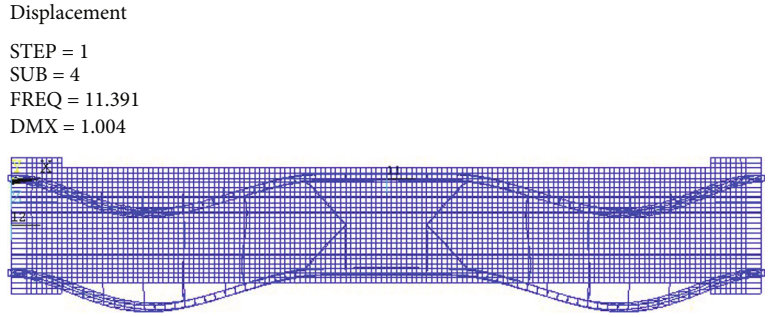

Figure 25: The fourth order buckling mode of arch bridge under case 7.

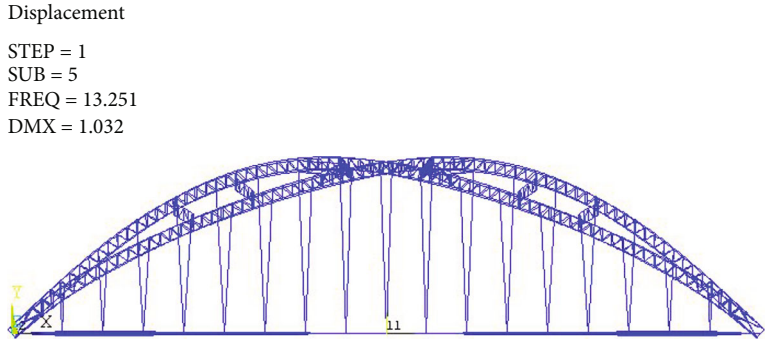

Figure 26: The fifth order buckling mode of arch bridge under case 7.

The overall displacement cloud maps of the arch bridge under cases 1, 2, 5, and 7 are shown in Figures 12–15.

We can see from Figures 12–15, under case 1, that the maximum displacement occurred near the middle span of the lower arch rib on the north side, and the maximum displacement is 5.39 cm; the deformation gradually decreased from the middle span to the bridge head and tail, showing along longitudinal and transverse symmetry. Under case 2, the maximum displacement of the arch bridge occurs near the middle of the fourth span of the south lane, and the maximum displacement is 5.22 cm, because the load applied is symmetrical along the longitudinal direction, while the transverse direction of the bridge is antisymmetric, the deformation gradually decreases from the middle span to the bridge head and tail, while the deflection increases significantly in the transverse direction where there is load. Under case 5, the maximum displacement of the arch bridge is 5.51 cm, which appears at the connection point between the horizontal beam and the hanger in the midspan; the deflection increases significantly in the place where there is load on the transverse bridge deck. Under case 7, the maximum displacement of the arch bridge is 5.72 cm, which occurs in the middle span of the arch rib on the south side, and it is less than the allowable deflection of the bridge $L/800 = 18.5$ cm.

5. Overall Stability Analysis of Arch Bridge

By analyzing the overall stability of the CFST arch bridge, the instability modes of the arch bridge under various cases are obtained. The internal force of the hanger calculated under cases 1 and 7 is equivalent to the external force and directly added to the lifting point on the upper arch rib, and the first

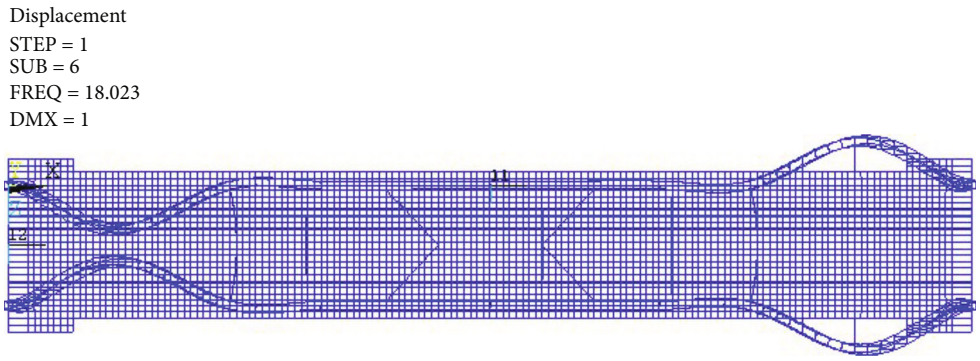

Figure 27: The sixth order buckling mode of arch bridge under case 7.

Table 1: The first six order stability coefficients of the main arch under various cases.

Buckling order	Stability coefficients						
	Case 1	Case 2	Case 3	Case 4	Case 5	Case 6	Case 7
1	4.9331	4.5693	4.5695	4.4062	4.2549	4.4732	4.0938
2	9.9988	9.2708	9.2891	8.9646	8.6754	9.0505	8.3450
3	10.931	10.158	10.141	9.7897	9.4517	9.9691	9.0945
4	13.635	12.671	12.677	12.243	11.842	12.396	11.391
5	15.935	14.758	14.778	14.249	13.773	14.417	13.251
6	21.548	19.766	20.021	19.248	18.734	19.074	18.023

six order buckling modes of the arch bridge under cases 1 and 7 are calculated, as shown in Figures 16–27.

We can see from Figures 16–21 that the first order buckling load coefficient is 4.9331, and the first, second, and fourth order buckling modes of the main arch are all out-of-plane instability; the specific modes can be divided into the first symmetrical buckling outside the arch rib plane, the second antisymmetric buckling outside the arch rib plane, and the symmetric buckling outside the arch rib plane. The sixth mode is the local antisymmetric buckling outside the rib surface near the arch foot, the third mode is antisymmetric buckling in the rib plane, and the fifth mode is torsional buckling of arch ribs. In general, for the arch bridge, considering the combined action of the arch rib, suspender, and deck system, the in-plane stiffness is larger. The out-of-plane stiffness decreases with the increase of the span, and the out-of-plane stability problem is more prominent than the in-plane stability problem. The above calculation results also fully reflect the stability characteristics of the CFST arch bridge.

We can see from Figures 22–27 that the first order buckling load coefficient is 4.0938, which is larger than the reduction in case 5. All the other modes of the arch are out-of-plane buckling except the third mode, which is in-plane buckling. The specific modes include the first symmetrical buckling outside the arch rib plane, the second antisymmetric buckling outside the arch rib plane, the fourth symmetrical buckling outside the arch rib plane, the fifth antisymmetric buckling outside the arch rib plane (torsion of the arch rib), and the local antisymmetric buckling outside the arch rib plane near the foot of the arch. These can reflect that the arch bridge outside the plane buckling problem is more prominent.

The first six order stability coefficients of the main arch under various cases are shown in Table 1. The stability coefficient refers to the application of unit load under various cases; the ratio of actual buckling load to unit load is the stability coefficient.

We can see from Table 1 that with the increase of the load, the stability coefficient of the main arch decreases gradually; that is, the stability safety reserve capacity decreases. With the increase of the buckling order, the stability coefficient gradually increases; that is to say, the possibility of high-order buckling becomes less and less. With the increase of the instability order, the stability coefficient changes more and more obviously with the load. For example, in the first instable mode, the stability coefficient of case 1 and case 2 varies by 0.3638; in the sixth instable mode, the stability coefficient of case 1 and case 2 varies by 1.782. The stability coefficients of different modes in case 2 and case 6 are very small, so the crowd load has little influence on the stability of the arch bridge.

6. Conclusion

(1) The main deformation of the arch bridge is the vertical displacement of the bridge deck; the axial force of most members of the upper arch rib is greater than that of the lower arch rib

(2) The axial force and bending moment of the lower arch rib near the arch foot are larger, which first enters the plastic state, and the stiffness should be strengthened in the structural design

(3) The maximum compressive stress appears near the arch foot, and the maximum compressive stress is less than the compressive strength of concrete; the arch bridge meets the strength requirements

(4) The maximum vertical displacement of the arch bridge is 5.72 cm, the displacement value is small, and the bridge meets the stiffness requirements

(5) The hanger axial force is symmetrically distributed, and the hanger axial force at the bridge middle span

and ends is large, while that on the other hanger has little change

(6) The vertical stiffness of the arch bridge is greater than the lateral stiffness, and the basic instability of the arch bridge is out-of-plane. The lateral support should be strengthened; it increases the lateral stiffness of the arch bridge and the ultimate bearing capacity of the main arch

Data Availability

The data used to support the findings of this study are included within the article.

Ethical Approval

The content of the thesis conforms to the moral and ethical standards. Review of essays ensures independence and fairness. The data in this paper are real and reliable, and there is no plagiarism. The paper was not duplicated. The references are in accordance with the standard.

Conflicts of Interest

There is no conflict of interest in funding, intellectual property rights, personal relationships, ideology, and academic nature. This paper was published without any conflict of interest with anyone other than the author.

Authors' Contributions

The authors of this paper are Yanli WU, Mowei QIU, Shaokun Ma, Xinlei Gao, and Yahong Han. All the authors have made scientific contributions to the results of the paper.

Acknowledgments

This paper is funded by the Cultivation Program for Young Backbone Teachers in Colleges and Universities of Henan Province (2020GGJS285) and Soft Science Research Project of Henan Province (222400410319). All thanks are due to those who contribute to this paper.

References

[1] W. Hai-jun, H. Li, W. Shao-rui, L. Jin-Quan, and L. Ping, "Geometry control method based on stress-free state theory for long-span concrete-fill steel tube arch bridge," *Bridge Construction*, vol. 50, no. 6, pp. 20–26, 2020.

[2] C. Guo and Z. Lu, "Effect of circumferential gap on dynamic performance of CFST arch bridges," *Journal of Bridge Engineering*, vol. 26, no. 2, 2021.

[3] D. Li Ji, Z. B. Xin, and L. Yan, "Sensitivity analysis of structural parameters of concrete-filled steel tube arch bridge with multiple arch ribs," *Journal of China & Foreign Highway*, vol. 40, no. 5, pp. 105–112, 2020.

[4] W. Li, Y. Lu-Song, L. Shi-Zhong, L. Zi-Qi, and L. Peng, "Seismic vulnerability analysis of irregular concrete-filled steel tube arch bridge under transverse seismic action," *Journal of Lanzhou Jiaotong University*, vol. 39, no. 5, pp. 13–19, 2020.

[5] W. Hao-Qi, Y. Jing, and W. Hai-long, "Calculation and analysis of unstressed length of suspender of concrete-filled steel tube arch bridge," *Engineering and Technological Research*, vol. 5, no. 16, pp. 241-242, 2020.

[6] Z. Siyuan and Y. Bo, "Study on structural stability and dynamic performance of concrete-filled steel tubular arch bridge with long span," *Journal of Safety Science and Technology*, vol. 18, no. 4, pp. 185–190, 2022.

[7] H. Feng and F. Yefei, "Stability analysis of arch rib grouting construction of concrete filled steel tube arch bridge," *Guangdong Architecture Civil Engineering*, vol. 27, no. 9, pp. 60–62, 2020.

[8] L. Fuzhong, L. Guangqi, and G. Baolin, "Analysis of in-plane stability parameters of single tube CFST arch bridge," *Shandong Communications Technology*, vol. 4, pp. 55–57, 2019.

[9] X. Weiwei, Y. Zhiquan, and Y. Lufeng, "Linear elastic iteration method for ultimate stability bearing capacity of concrete filled steel tubular arch bridge," *China Railway Science*, vol. 39, no. 1, pp. 39–48, 2018.

[10] W. Yuyin, L. Changyong, L. Yong, and Z. Sumei, "Nonlinear stability analysis and completed bridge test on slanting type CFST arch bridges," *Journal of Building Structures*, vol. 36, no. S1, pp. 107–113, 2015.

[11] S. Fuchun and W. Qianna, "Effects of crossbars on the lateral elastic stability of lift-basket CFST truss rib arch bridge," *Journal of Shenyang Jianzhu University(Natural Science)*, vol. 30, no. 5, pp. 850–855, 2014.

[12] B. Xue, X. Du, J. Wang, and X. Yu, "A scaled boundary finite-element method with B-differentiable equations for 3D frictional contact problems," *Fractal and Fractional*, vol. 6, no. 3, p. 133, 2022.

[13] X. Du, H. Fang, S. Wang, B. Xue, and F. Wang, "Experimental and practical investigation of the sealing efficiency of cement grouting in tortuous fractures with flowing water," *Tunneling and Underground Space Technology*, vol. 108, article 103693, 2021.

[14] D. Ma, D. Hongyu, Z. Jixiong, L. Xianwei, and L. Zhenhua, "Numerical simulation of water–silt inrush hazard of fault rock: a three-phase flow model," *Rock Mechanics and Rock Engineering*, vol. 55, no. 8, pp. 5163–5182, 2022.

[15] Q. Li, D. Ma, Y. Zhang, Y. Liu, and Y. Ma, "Insights into controlling factors of pore structure and hydraulic properties of broken rock mass in a geothermal reservoir," *Lithosphere*, vol. 2021, no. Special 5, article 3887832, 2021.

[16] X. Wei-wei, T. Rui-kai, Y. Zhi-quan, and T. Qiu-hong, "Automatic monitoring and control of initial stresses in steel tubes of concrete-filled steel tubular arch bridge," *World Bridges*, vol. 49, no. 1, pp. 83–88, 2021.

[17] Z. Qian, Z. Jian-ting, Z. Jia-cheng, and Z. Lan, "Self-regulating loading pouring method of long span CFST arch bridge," *Journal of Harbin Institute of Technology*, vol. 52, no. 3, pp. 82–89, 2020.

[18] S. Heng-li, J. Ri-chen, Z. Yu-zhu, and S. Teng-fei, "Analysis of tensioning scheme of hanger of concrete filled steel tubular tied arch bridge," *Communications Science and Technology Heilongjiang*, vol. 42, no. 6, pp. 102–105, 2019.

[19] J. Jian-Jing, L. Xin-Zheng, and Y. Lie-Ping, *Finite Element Analysis of Concrete Structures*, Tsinghua University Press, 2004.

[20] G. Shu-Guang and X. Gui-Lan, *ANSYS Operating Commands and Parameterized Programming*, Machinery Industry Press, 2004.